

Single-shot holography for depth resolved three dimensional imaging

Nektarios Koukourakis^{1,*}, Christoph Kasseck¹, Daniel Rytz²
Nils C. Gerhardt¹ and Martin R. Hofmann¹

¹Photonics and Terahertz-Technology, Ruhr-University Bochum, Universitätsstr. 150,44780 Bochum, Germany

²FEE GmbH, Struthstr. 2, 55743 Idar-Oberstein, Germany

*Nektarios.Koukourakis@rub.de

Abstract: We introduce a method for depth-resolved photorefractive holographic imaging with potentially extremely short acquisition time for a complete three dimensional (3D) image. By combining the advantages of full-field frequency-domain optical coherence tomography with those of photorefractive holography our concept is capable of obtaining 3D information with only one single shot. We describe the operation principle of our concept and give a first experimental proof of principle.

©2009 Optical Society of America

OCIS codes: (090.4220) Multiplex holography; (090.7330) Volume gratings;(190.5330) Photorefractive optics; (170.4500) Optical coherence tomography; (070.4790) Spectrum analysis; (100.2650) Fringe analysis; (090.1995) Digital Holography.

References and links

1. C. Dunsby, and P. M. W. French, "Techniques for depth-resolved imaging through turbid media including coherence-gated imaging," *Appl. Phys. (Berl.)* **36**, 207–227 (2003).
2. D. Huang, E. A. Swanson, C. P. Lin, J. S. Schuman, W. G. Stinson, W. Chang, M. R. Hee, T. Flotte, K. Gregory, C. A. Puliafito, "Optical coherence tomography," *Science* **254**(5035), 1178–1181 (1991).
3. C. A. Puliafito, M. R. Hee, C. P. Lin, E. Reichel, J. S. Schuman, J. S. Duker, J. A. Izatt, E. A. Swanson, and J. G. Fujimoto, "Imaging of macular diseases with optical coherence tomography," *Ophthalmology* **102**(2), 217–229 (1995).
4. J. G. Fujimoto, "Optical coherence tomography for ultrahigh resolution in vivo imaging," *Nat. Biotechnol.* **21**(11), 11361 (2003).
5. G. J. Tearney, M. E. Brezinski, B. E. Bouma, S. A. Boppart, C. Pitris, J. F. Southern, and J. G. Fujimoto, "In vivo endoscopic optical biopsy with optical coherence tomography," *Science* **276**(5321), 2037–2039 (1997).
6. M. E. Brezinski, and J. G. Fujimoto, "Optical Coherence Tomography: High-Resolution Imaging in Nontransparent Tissue," *IEEE Sel. Top. Quantum Electron.* **5**(4), 1185–1192 (1999).
7. A. F. Fercher, C. K. Hitzenberger, G. Kamp, and S. Y. El-Zaiat, "Measurement of intraocular distances by backscattering spectral interferometry," *Opt. Commun.* **117**(1-2), 43–48 (1995).
8. A. F. Fercher, W. Drexler, C. K. Hitzenberger, and T. Lasser, "Optical coherence tomography- principles and applications," *Rep. Prog. Phys.* **66**(2), 239–303 (2003).
9. R. Leitgeb, C. K. Hitzenberger, and A. F. Fercher, "Performance of fourier domain vs. time domain optical coherence tomography," *Opt. Express* **11**(8), 889–894 (2003).
10. G. Häusler, and M. W. Lindner, "Coherence Radar and Spectral Radar- New Tools for Dermatological Diagnosis," *J. Biomed. Opt.* **3**(1), 21 (1998).
11. S. H. Yun, G. J. Tearney, J. F. de Boer, N. Iftimia, and B. E. Bouma, "High-speed optical frequency-domain imaging," *Opt. Express* **11**(22), 2953–2963 (2003).
12. A. M. Davis, M. A. Choma, and J. A. Izatt, "Heterodyne swept-source optical coherence tomography for complete complex conjugate ambiguity removal," *J. Biomed. Opt.* **10**(6), 064005 (2005).
13. M. A. Choma, M. V. Sarunic, C. Yang, and J. A. Izatt, "Sensitivity advantage of swept source and Fourier domain optical coherence tomography," *Opt. Express* **11**(18), 2183–2189 (2003).
14. P. H. Tomlins, and R. K. Wang, "Theory, development and applications of optical coherence tomography," *Appl. Phys. (Berl.)* **38**, 2519–2535 (2005).
15. E. Beaurepaire, A. C. Boccara, M. Lebec, L. Blanchot, and H. S. Jalmes, "Full-field optical coherence microscopy," *Opt. Lett.* **23**(4), 244 (1998).
16. B. Grajciar, M. Pircher, A. F. Fercher, and R. A. Leitgeb, "Parallel Fourier domain optical coherence tomography for in vivo measurement of the human eye," *Opt. Express* **13**(4), 1131 (2005).
17. A. V. Zvyagin, P. Blazkiewicz, and J. Vintrou, "Image reconstruction in full-field Fourier-domain optical coherence tomography," *J. Opt. A* **7**, 350–356 (2005).

18. K. A. Stetson, "Holographic fog penetration," *J. Opt. Soc. Am.* **57**(8), 1060–1061 (1967).
19. K. G. Spears, J. Serafin, N. H. Abramson, X. M. Zhu, and H. Bjelkhagen, "Chrono-coherent imaging for medicine," *IEEE Trans. Biomed. Eng.* **36**(12), 1210–1221 (1989).
20. N. Koukourakis, M. Breede, N. C. Gerhardt, M. Hofmann, S. Köber, M. Salvador, and K. Meerholz, "Depth resolved holographic imaging with variable depth resolution using spectrally tunable diode laser," *Electron. Lett.* **45**(1), 46 (2009).
21. U. Schnars, and W. P. O. Jüptner, "Direct recording of holograms by a CCD target and numerical reconstruction," *Appl. Opt.* **33**(2), 179–181 (1994).
22. U. Schnars, and W. P. O. Jüptner, "Digital recording and numerical reconstruction of holograms," *Meas. Sci. Technol.* **13**(9), R85–R101 (2002).
23. H. Chen, M. Shih, E. Arons, J. Lopez, D. Dilworth, and P. C. Sun, "Electronic holographic imaging through living human tissue," *Appl. Opt.* **33**(17), 3630 (1994).
24. K. Jeong, J. J. Turek, and D. D. Nolte, "Fourier-domain digital holographic optical coherence imaging of living tissue," *Appl. Opt.* **46**(22), 4999–5008 (2007).
25. M. C. Potcoava, and M. K. Kim, "Optical tomography for biomedical applications by digital interference holography," *Meas. Sci. Technol.* **19**(7), 074010 (2008).
26. P. Yu, M. Mustata, P. M. W. French, J. J. Turek, M. R. Melloch, and D. D. Nolte, "Holographic optical coherence imaging of tumor spheroids," *Appl. Phys. Lett.* **83**(3), 575–577 (2003).
27. P. Yu, M. Mustata, L. Peng, J. J. Turek, M. R. Melloch, P. M. W. French, and D. D. Nolte, "Holographic optical coherence imaging of rat osteogenic sarcoma tumor spheroids," *Appl. Opt.* **43**(25), 4862–4873 (2004).
28. S. C. W. Hyde, N. P. Barry, R. Jones, J. C. Dainty, P. M. W. French, M. B. Klein, and B. A. Wechsler, "Depth-resolved holographic imaging through scattering media by photorefractive," *Opt. Lett.* **20**(11), 1331 (1995).
29. Z. Ansari, Y. Gu, J. Siegel, D. P. Karavassilis, C. W. Dunsby, M. Itoh, M. Tziraki, R. Jones, P. M. W. French, D. D. Nolte, W. Headley, and M. R. Melloch, "High Frame-Rate, 3-D Photorefractive Holography Through Turbid Media With Arbitrary Sources, and Photorefractive Structured Illumination," *IEEE J. Sel. Top. Quantum Electron.* **7**(6), 878 (2001).
30. D. Psaltis, M. Levene, A. Pu, G. Barbastathis, and K. Curtis, "Holographic storage using shift multiplexing," *Opt. Lett.* **20**(7), 782 (1995).
31. W. J. Carlsen, "Holographic Page Synthesis for Sequential Input of Data," *Appl. Opt.* **13**(4), 896 (1974).
32. C. Denz, K.-O. Müller, T. Heimann, and T. Tschudi, "Volume holographic Storage demonstrator based on Phase-coded multiplexing," *IEEE J. Sel. Top. Quantum Electron.* **4**(5), 832 (1998).
33. F. H. Mok, M. C. Tackitt, and H. M. Stoll, "Storage of 500 high-resolution holograms in a LiNbO₃ crystal," *Opt. Lett.* **16**(8), 605 (1991).
34. G. A. Rakuljic, V. Leyva, and A. Yariv, "Optical data storage by using orthogonal wavelength-multiplexed volume holograms," *Opt. Lett.* **17**(20), 1471 (1992).
35. M. G. Littman, "Single-mode operation of grazing-incidence pulsed dye laser," *Opt. Lett.* **3**(4), 138–140 (1978).
36. J. M. Schmitt, "Optical Coherence Tomography (OCT): A Review," *IEEE J. Sel. Top. Quantum Electron.* **5**(4), 1205–1215 (1999).
37. M. Born, and E. Wolf, VII Theory of interference and interferometers," in *Principles of Optics*, (Cambridge University Press, 7th edition, (1999).
38. M. Wojtkowski, A. Kowalczyk, R. Leitgeb, and A. F. Fercher, "Full range complex spectral optical coherence tomography technique in eye imaging," *Opt. Lett.* **27**(16), 1415 (2002).
39. J. Zhang, J. S. Nelson, and Z. Chen, "Removal of a mirror image and enhancement of the signal-to-noise ration in Fourier-domain optical coherence tomography using an electro-optic phase modulator," *Opt. Lett.* **30**(2), 147 (2005).
40. R. K. Wang, "Fourier domain optical coherence tomography achieves full range complex imaging in vivo by introducing a carrier frequency during scanning," *Phys. Med. Biol.* **52**(19), 5897–5907 (2007).
41. H. Kogelnik, "Coupled Wave Theory for Thick Hologram Gratings," *Bell Syst. Tech. J.* **48**, 9 (1969).
42. F. Zhao, H. Zhou, S. Yin, and F. T. S. Yu, "Wavelength-multiplexed holographic storage by using the minimum wavelength channel separation in a photorefractive crystal fiber," *Opt. Commun.* **103**(1-2), 59–62 (1993).
43. S. Campbell, Y. Zhang, and P. Yeh, "Writing and copying in volume holographic memories: approaches and analysis," *Opt. Commun.* **123**(1-3), 27–33 (1996).
44. W. J. Burke, and P. Sheng, "Crosstalk noise from multiple thick-phase holograms," *J. Appl. Phys.* **48**(2), 681 (1977).
45. K. Peithmann, A. W. K. Buse, "Incremental recording in lithium niobate with active phase locking," *Opt. Lett.* **23**(24), 1927 (1998).
46. A. C. Strasser, E. S. Maniloff, K. M. Johnson, and S. D. D. Goggin, "Procedure for recording multiplex exposure holograms with equal diffraction efficiency in photorefractive media," *Opt. Lett.* **14**(1), 6 (1989).
47. J. E. Ford, Y. Fainman, and S. H. Lee, "Enhanced photorefractive performance from 45°-cut BaTiO₃," *Appl. Opt.* **28**(22), 4808 (1989).
48. M. Chi, S. Dou, H. Gao, H. Song, J. Zu, Y. Zhu, and P. Ye, "Enhanced Photorefractive Properties of a Rh-Doped BaTiO₃ Crystal at Elevated Temperature," *Chin. Phys. Lett.* **14**(11), 838–841 (1997).
49. A. A. Grabar, I. V. Kedyk, M. I. Gurzan, I. M. Stoika, A. A. Molnar, and Y. M. Vysochanskii, "Enhanced photorefractive properties of modified Sn₂P₂S₆," *Opt. Commun.* **188**(1-4), 187–194 (2001).

1. Introduction

Three dimensional optical imaging through turbid or scattering media is of great interest for numerous applications, in particular for biomedical imaging. In conventional optical imaging approaches scattering media, such as biological tissue, are illuminated with near infrared (NIR) radiation in their transparency window and the information bearing ballistic light is filtered out of the scattered light background by coherence gating [1]. The most prominent concept is optical coherence tomography (OCT) [2]. OCT is a non-invasive, cross-sectional imaging technique that measures depth-resolved reflectance of scattering media. OCT is based on low-coherence interferometry and has already been established in several clinical applications [3–5]. There are two different approaches to OCT called time-domain OCT (TD-OCT) and frequency-domain OCT (FD-OCT).

In TD-OCT the reference arm of a Michelson interferometer is scanned. As interference only appears if the travel path lengths of reference and object beams are matched within the coherence length of the light source, the scan collects the depth-information [2,6]. As the acquisition takes place pointwise, two additional lateral scans are needed to obtain a complete 3D data set. As biomedical imaging is very sensitive to motion artefacts, it requires fast data acquisition and therefore it is desirable to reduce the number of scans and the acquisition time of the data as much as possible. In FD-OCT the depth information is obtained by analysis of the spectrum of the backscattered light [7,8]. That makes the mechanical depth-scan, that appears in TD-OCT, superfluous, but still requires two lateral scans and additional wavelength-scanning. Depending on the used laser source and detector, two variations of FD-OCT are classified. Spectral-domain OCT (SD-OCT) [9,10] (or spectral-radar) utilizes a broadband source and a spectrometer. In the so called swept source-OCT [11,12] (SS-OCT) a rapidly tuned broadband source and an integrating detector are used. As it was shown FD-OCT has the advantage of an improved sensitivity [9,13,14] in comparison to TD-OCT. But as still lateral scans are needed all described OCT techniques have been extended to full-field (FF) detection to get even faster data acquisition. In FF-OCT detector arrays are used, that record 2D-interference fringes and thus make the need of lateral scans superfluous [15–17].

Holography is a closely related technique to OCT that is also based on interference and thus provides the possibility to apply coherence gating. Accordingly several techniques in the holographic field use similar approaches like OCT. The first holographic coherence gating was introduced by Stetson [18] for imaging through fog. Afterwards light-in-flight holography was used with a short coherence laser to obtain depth-resolved images of 3D objects [19], opening up the field of depth resolved holographic imaging (DRHI). DRHI allows the recording of complete two dimensional image planes in each holographic storage process and requires scanning in the depth direction only. In DRHI, like in TD-OCT, the achievable depth resolution is inversely proportional to the coherence length of the light-source. If a very short coherence length is used, the resolution is very high but the scanning need is increased compared to a long coherent laser, as more images must be recorded to correctly sample the image volume. We recently showed that a tunable laser allows controlling the coherence length of a DRHI system by changing its tuning width [20]. This raises the possibility to change the depth-resolution of the system dynamically and to realise zooming. A scan with a long coherence length can be used to find the area of interest quickly and afterwards, only by changing the tuning width, a better resolution can be used for more detailed imaging. Using this zooming option reduces the overall scanning requirement, but still needs mechanical scanning that is time consuming.

In the first holographic coherence gating experiments, mentioned above [18,19], static holograms were used, that had to be exposed and developed afterwards. This prohibited the desirable real-time acquisition, that relies on continuously updatable dynamic holographic

media like charge coupled device (CCD) chips or photorefractive materials. In digital holography (DH) the interference patterns are recorded by CCD chips and the reconstruction is performed numerically [21,22]. But DH, like holographic films, suffers from saturation effects caused by the incoherent background. Nevertheless DH has been applied for imaging in tissue and has grown to a powerful discipline [23–25]. Photorefractive holography has the advantage that the background of scattered light is removed during recording, as only the spatial derivative of the incident light intensity creates the holographic grating while the integrated intensity does not affect the grating. Photorefractive holography has recently been used for optical coherence imaging in living tissue, where rat osteogenic tumor spheroids were imaged [26,27]. Several photorefractive materials have been developed and have been used in DRHI like photorefractive crystals, multiple quantum wells or polymers [20,28,29]. Photorefractive crystals offer the possibility to superimpose several holograms in the same medium and reconstruct each of them independently without any distortion by one of the others. This unique feature called multiplexing, has been realized with several different methods, such as shift multiplexing [30], spatial multiplexing [31], phase-coded multiplexing [32], angular multiplexing [33] or wavelength multiplexing [34].

In this paper we introduce a new approach for single-shot three dimensional imaging. Our concept combines the advantages of photorefractive DRHI and full-field swept-source OCT (FF-SS-OCT). In contrast to traditional DRHI with short coherent sources that requires scanning of the reference arm to get the depth-information, we use a comb of wavelengths, with each wavelength having a long coherence length. The hologram written with a long coherence length reconstructs a greater depth of the sample, in comparison to common DRHI, as the depth resolution is inversely proportional to the coherence length. Instead of depth-scanning we use the FF-SS-OCT approach to resolve the sample depth. Therefore wavelength multiplexing is used to store a set of object beams simultaneously in a photorefractive medium. Thus our concept allows three-dimensional image information to be stored during a single laser shot, without any moving parts and with no need of scanning. In this paper we discuss the theoretical background for obtaining 3D image information from these full-field SS-OCT data and give an experimental proof of principle.

2. Experiments

Our proof of principle studies consist of three important steps. We start with the realization of a FF-SS-OCT setup to prove that we are able to extract the depth-information from the acquired data set. The second step is to introduce holographic storage into the setup and to sequentially store each object beam in a hologram and after read-out to use a similar approach like FF-SS-OCT for evaluation. The last step of our proof of principle studies aims at the improvement of the storage capability of our system. We use sequential wavelength multiplexing of three holograms during each recording to prove that the multiplexing ability of photorefractive materials bears the possibility to record a data set, that allows reconstruction of a complete 3D object, within one single-shot

2.1 Full-field swept-source optical coherence tomography (FF-SS-OCT)

The first setup is shown in Fig. (1). Our light source is an external-cavity tunable diodelaser in Littman [35] configuration, which we used already in earlier experiments [20]. The laser emits one narrow laser line at a time and can be easily tuned over a range of about 40 nm around the center wavelength of about 820 nm, by rotation of the external cavity mirror.

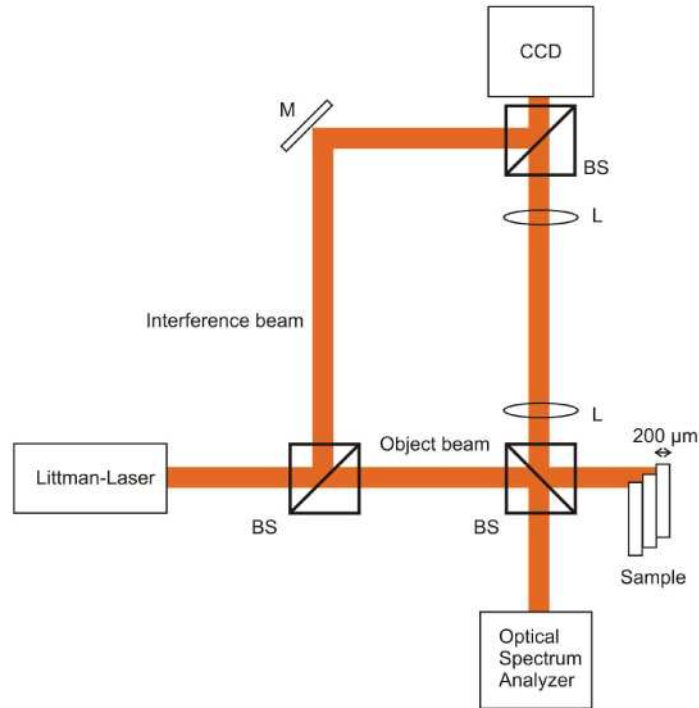


Fig. 1. FF-SS OCT setup (BS: beamsplitter, M: mirror, L: lens).

The light is divided by a 50:50 beam splitter into object- and interference-beams. The object beam is directed onto a three dimensional model sample consisting of a stack of polished aluminium platelets arranged as stairs with each step being $200\ \mu\text{m}$ high Fig. (2).

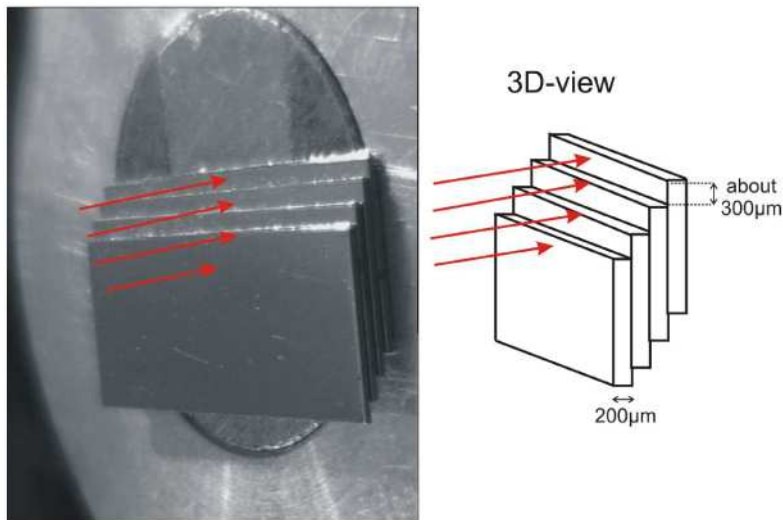


Fig. 2. Photo (left) and schematic (right) of model sample, consisting of a stack of polished Al-platelets arranged as stairs with each step being $200\ \mu\text{m}$ high. The light is normally incident (indicated by the arrows).

A second beam splitter is used to ensure that the light is normally incident on the sample where it is reflected and then led towards the CCD-chip by the beam splitter. Another beam

splitter completes the Mach-Zehnder Interferometer and combines object and reference beams.

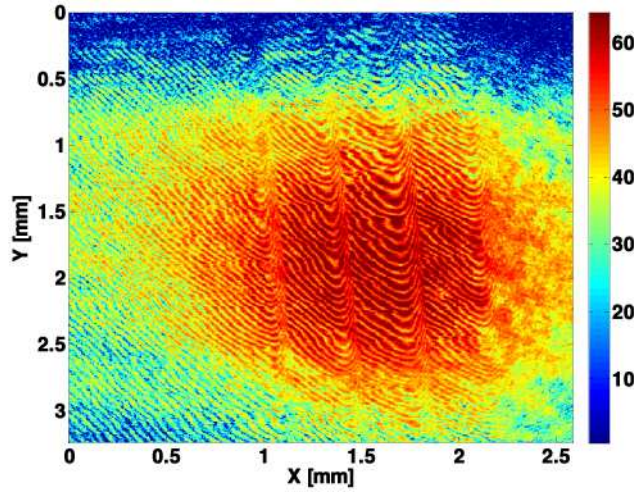


Fig. 3. Interference pattern recorded with FF-SS-OCT setup.

A CCD chip of 1376 x 1040 pixel with a pixel size of 6.45 μm x 6.45 μm is used for acquisition of the resulting interference patterns (Fig. (3)). The bandwidth that is needed to resolve two steps of the sample, is calculated using Eq. (1) [36],

$$\Delta\lambda = 0.44 \frac{\lambda_0^2}{\Delta z} \quad (1)$$

where $\Delta\lambda$ is the full width at half maximum of the required spectrum, λ_0 is the central wavelength and Δz the height of one aluminium platelet. As this formula implies a Gaussian spectrum, and our source does not have a Gaussian shape, the result of Eq. (1) provides only a rough estimation. Choosing $\lambda_0=820$ nm and $\Delta z=200$ μm we obtain a required bandwidth of $\Delta\lambda = 1.48$ nm. As the sample consists of 4 platelets, each being 200 μm high, the depth that has to be resolved is $h = (4 \cdot 200 \mu\text{m} + d)$, with d being the path length difference between object and reference arm Fig. (4). The theoretical minimum tuning-stepwidth of the wavelength can thus be estimated using Eq. (2) [37].

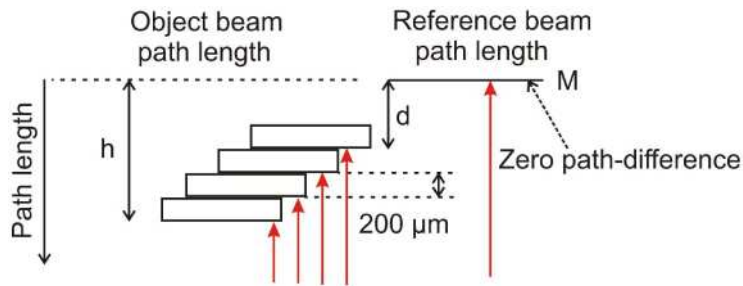


Fig. 4. Path lengths of object and reference beam. The arrows show the light incidence.

$$\Delta\lambda_{\text{step}} = \frac{\lambda_0^2}{2h} \quad (2)$$

Choosing $d = 200$ μm leads to the minimal step-width $\Delta\lambda_{\text{step}}=0.336$ nm.

For our experiments we choose a bandwidth between 4 nm and 8 nm with a step-width of 0.1 nm. Both a broader bandwidth and a smaller step-width lead to improved resolution in the reconstructed image. We acquire 80 interference patterns sequentially, using 80 wavelengths, spread over 8 nm (821.0 nm...829.0 nm) bandwidth in 0.1 nm steps.

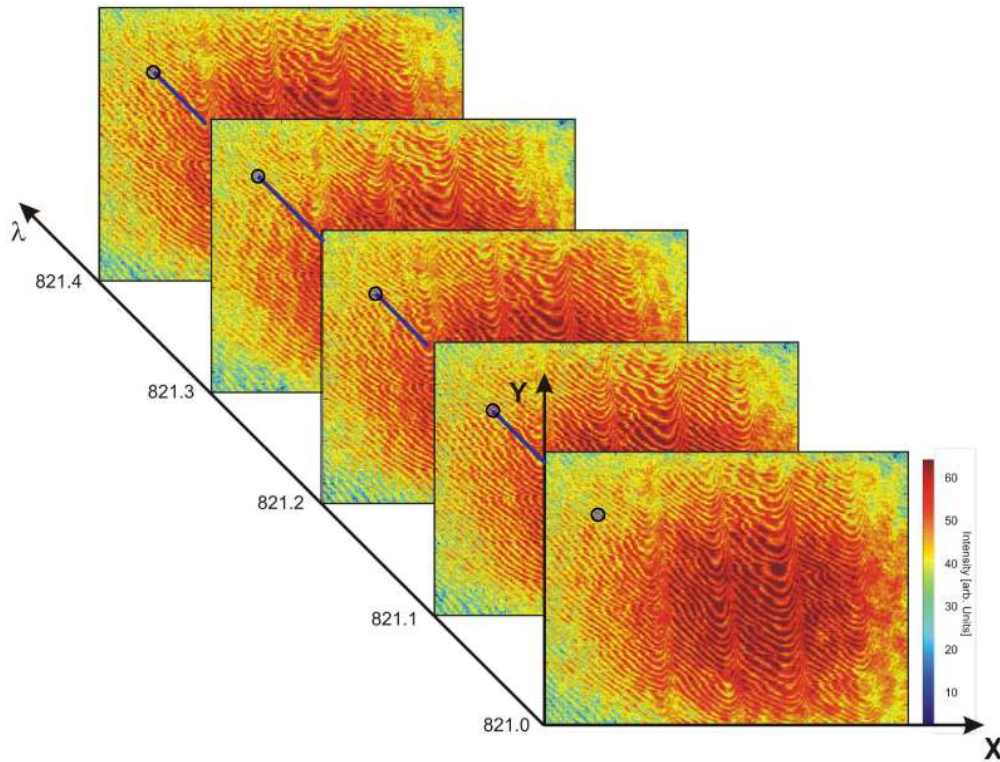


Fig. 5. The 4D-data set is resorted. The intensity modulation over wavelength, e.g. at the marked pixel position, is analyzed.

The interference pattern is a 3D data cube consisting of 2 lateral dimensions (x, y) and the encoded intensity dimension I (color in Fig. (3)). Hence, considering the wavelength dimension, the full data set is 4 dimensional (x, y, I, λ) (Fig. (5)). For evaluation the wavelength dependent intensity distribution at each pixel-position (x_i, y_j, I, λ) is analyzed. An example is shown in Fig. (6). This resulting intensity modulation is inversely Fourier-transformed in order to obtain the depth-profile at the respective pixel-position. By repeating this for all CCD-pixels the complete depth-profile of the sample can be reconstructed. The expected result can be recognized in Fig. (4). The position of the mirror sets the reference plane. The difference of the reference path length and the path length to a certain step of the sample leads to a certain modulation in the spectrum. The result will show the path length difference between the mirror and the steps of the sample.

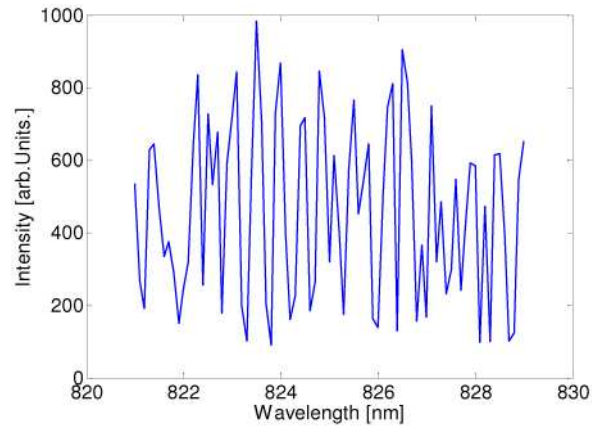


Fig. 6. The intensity modulation over wavelength at pixel-position (400,300).

The resulting image, after evaluation, is shown in Fig. (7). The vertical axis shows the path length difference between object and interference arm and thus resolves the depth-information of the sample. The steps can be clearly distinguished and the reconstructed length scales agree with those of the sample. It is to mention that FF-SS-OCT data processing suffers from several problems, so that the reconstructed images contain some artefacts apart

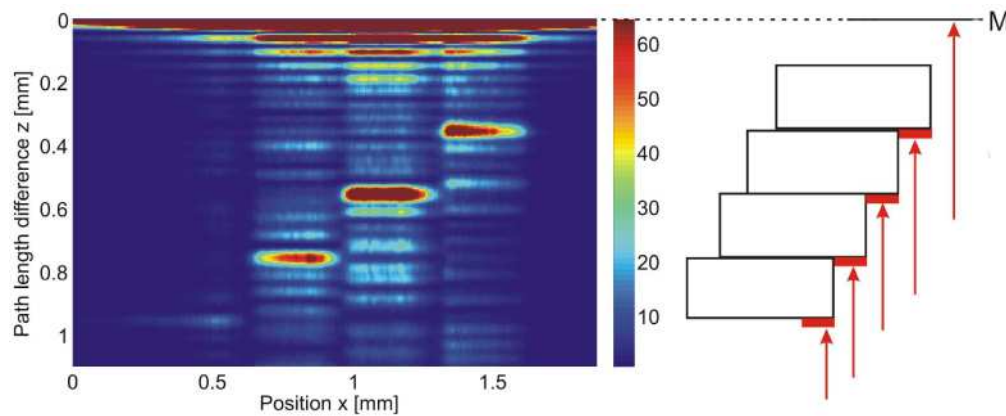


Fig. 7. Reconstructed FF-SS-OCT image (left), drawing of the sample (right).

from the main image information. One artefact is created by the data processing, as the Fourier transformation of the superimposed dc terms lead to the very strong signal at $z=0$. Another artefact is due to the fact that the Fourier transformation of a real function has Hermitian symmetry. This leads to complex conjugate artefacts, which are positioned symmetrically to the true image on the other side of the zero-phase delay line. This limits the measurement depth range, as only half the complex space can be utilized for imaging, because it has to be ensured, that the true and mirror image do not overlap. It is desirable to place the zero-phase delay inside of the sample because the sensitivity of FD-OCT systems is the highest there and drops off along the depth. The mirror image makes this impossible. It gets even worse, because the very strong dc term forces one to move the sample away from the zero-phase delay (d in Fig. (4)). These problems have been recognized earlier by other groups and can be solved [38–40]. However, here we concentrate on our proof of principle studies and do not implement correction schemes for those artefacts.

2.2 FF-SS-OCT with sequential holographic storage

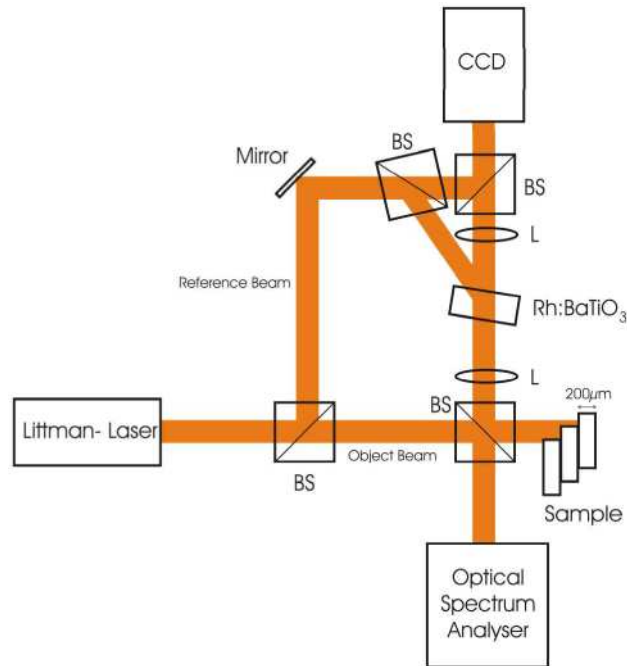


Fig. 8. Single-shot setup (BS: beamsplitter, M: mirror, L: lens).

For the second step holographic storage is introduced to the experiment. Now the heart of the setup consists of two nested Mach-Zehnder Interferometers (Fig. 8). The photorefractive medium we use is a 0°-cut Rh:BaTiO₃ crystal, grown by the FEE GmbH, having dimensions of 7.5 mm, 1.9 mm, 8.0 mm (=c axis) and 1000 ppm Rhodium in the melt. Another beam splitter is introduced, that divides the interference beam into two parts. One part is still the interference beam, while the second part is named reference beam as usual in holography. The beams coming from the sample and reference arms interfere within the crystal and create a reflection grating via the photorefractive effect. The crystal is placed between two lenses with a focal length of $f=150$ mm each, forming a 4f-geometry and thus recording Fourier-holograms. The angle between the writing beams is about 160° in air, which leads to a grating period of $\Lambda=0.4$ μm in the crystal. The crystal is slightly tilted, so that the object beam and the normal of the crystal enclose a 15° angle. This geometry is chosen because the diffracted intensity has a maximum for this configuration. Both beams are p-polarized, in order to make use of the largest electro-optic coefficient r_{42} of the BaTiO₃ crystal oriented such that its c-axis lies in the plane of incidence. After the hologram is written, a computer driven mechanical shutter blocks the object beam. Now the reference beam is diffracted from the reflection grating and reconstructs the object beam. The reconstructed object beam and the interference beam are combined by the beam splitter and the resulting interference patterns are recorded by the camera, similar to the foregoing experiment. The important difference to the FF-SS-OCT experiment is, however, that the object beam is intermediately stored within a hologram.

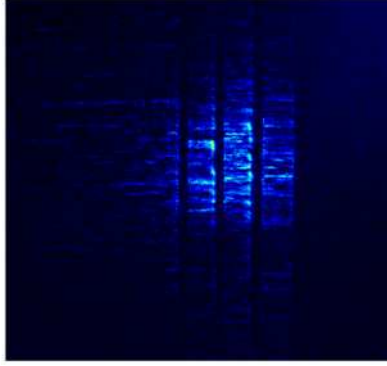


Fig. 9. Reconstructed hologram, before it interferes with the interference beam.

The photorefractive crystal is operated at 22°C. The write and erase times are both set at 45 s. This time is surely too long, but in the course of this paper it will be explained how the writing time can be decreased, and for the first studies it is sufficient. We start the experiment with the recording and reconstruction of a hologram. As the coherence length of our source is long enough, all steps of the sample are reconstructed simultaneously and can be clearly recognized, but without any depth information Fig. (9). As mentioned, common DRHI uses a short coherence length and depth scanning to achieve the depth resolution. To overcome the need of depth-scanning we use the principle of FF-SS-OCT to retrieve the depth information.

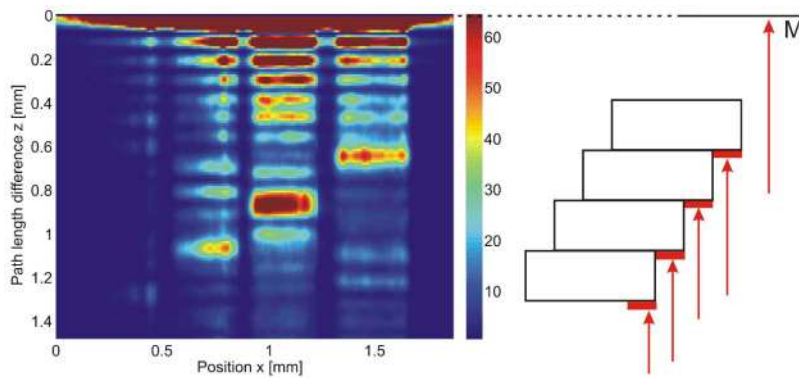


Fig. 10. Reconstructed image with sequentially recorded and readout holograms (left). Sample (right).

The first hologram in our experiment is recorded and read out at 818 nm. After the resulting interference patterns are acquired the hologram is erased and the laser is tuned to 818.1 nm so that the procedure can begin again. 40 wavelengths are used to record 40 holograms sequentially. Thus 40 interference patterns are obtained. The data is analysed as described above and the resulting image is shown in Fig. (10). Again the different steps can be clearly distinguished and the step-height corresponds to that of the sample, although the image resolution is decreased due to the reduced number of wavelengths used, in comparison to Fig. (7). As expected, the image contains the same artefacts as Fig. (7). But apart from that, the result clearly demonstrates the capability to extract depth resolved information from hologram sequences with different wavelengths. This result is an additional information to the reconstructed hologram and makes the obtained data three dimensional.

In our third step wavelength multiplexing is introduced to our experiment and thus the storage capability of the system is improved.

2.3 FF-SS-OCT with sequentially multiplexed holographic storage

As multiplexing techniques in photorefractive holography may suffer from cross-talk noise we first theoretically consider the required experimental conditions.

According to the coupled-wave theory introduced by Kogelnik [41], the diffraction efficiency of a phase reflection grating is described by Eq. (3)

$$\eta_B = \tan^2 \left(\frac{\pi \Delta n d}{\lambda \cos \theta_B} \right) \quad (3)$$

where d is the grating thickness in the photorefractive medium, λ is the wavelength, θ_B is the Bragg-angle and Δn is the amplitude of the refractive index modulation. As reflection gratings have a very small grating period, compared to transmission gratings, which leads to an increased wavelength selectivity, they are preferably used for wavelength multiplexing. It was shown that a counterpropagating setup shows the best performance for wavelength multiplexing [34]. When two holograms are written at two particular wavelengths, a slightly mismatched wavelength during read out of one hologram may possibly lead to reconstruction of both holograms. The diffraction efficiency for the Bragg-mismatched case is given by Eq. (4) where λ_B is the Bragg matched wavelength and $\Delta\lambda$ is the so called detuning

$$\eta = \eta_B \sin^2 \left(\frac{\lambda_B - \lambda}{\Delta\lambda} \right) \quad (4)$$

parameter, the diffraction efficiency drops the more the readout wavelength λ is detuned from the Bragg-case. The superposition of these undesired reconstructions is known as cross-talk noise, which can possibly lead to a degraded image quality of the desired hologram and should therefore be reduced. The diffraction efficiency reaches its first zero for a readout wavelength

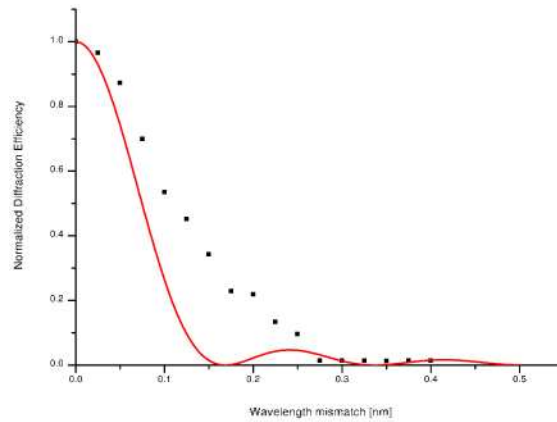


Fig. 11. Theoretical (solid line) and experimental (dotted curve) normalized diffraction efficiency as a function of Bragg mismatch for wavelength multiplexing

detuning of $\lambda = \lambda_B \pm \Delta\lambda$. Therefore the detuning parameter can be considered as the minimum wavelength channel separation one should use for wavelength multiplexing, as long as the linewidth of the laser is small enough [42]. The ideal laser source for wavelength multiplexing thus emits a comb of wavelengths with a minimum wavelength channel separation equal to the detuning parameter and provides a linewidth that is much smaller than the half width of the diffraction efficiency curve.

Combining the photorefractive wavelength multiplexing ability of a comb laser with the FD-OCT signal processing, enables three-dimensional image information to be stored with

one single laser shot. It should be noted that the read out of the hologram and the evaluation of the digital data may last considerably longer. But most applications require a short image acquisition time only, in order to avoid motion artifacts, and do not suffer from a more time consuming readout. Due to the lack of a laser source emitting a comb of wavelengths simultaneously we perform the proof of principle experiments with our tunable semiconductor laser. The main difference between our tunable laser and a comb source is that in case of the comb laser, the holograms are recorded simultaneously, whereas the holograms are written sequentially with a tunable source. As it was derived in [43], both multiplexing approaches theoretically lead to the same results, as they need exactly the same time to achieve exactly the same modulation of the refractive index. Also the degree of the index modulation is equal in both cases and can be calculated by Eq. (5), where Δn_n is the diffraction efficiency of the n-th hologram, Δn_{sat} is the saturation value of the refractive index and N is the number of multiplexed holograms.

$$\Delta n_n = \frac{\Delta n_{sat}}{N} \quad (5)$$

Accordingly our tunable source will lead to comparable results as a comb source would do. Nevertheless sequential writing has the disadvantage that the recording of a hologram partially erases the previously written holograms, which leads to highly non-uniform diffraction efficiencies of the multiplexed holograms. As it is desirable that the diffraction efficiencies for all multiplexed holograms are similar, several recording schedules have been developed that address this problem of sequential writing. A widely used approach is reducing the exposure time of subsequent holograms [44]. Another possibility for multiplexing uses incremental recording [45,46], where the holograms are recorded using a series of exposures that are shorter than the materials response time. For our proof of principle studies we use a simple approach of decreasing writing times for the subsequent holograms.

At first we measure the diffraction efficiency. For that purpose a hologram is written using a certain wavelength ($\lambda=820$ nm in our case). The reconstruction is performed using the same wavelength and the reconstructed hologram is acquired by the CCD chip. A rectangular part of the reconstructed hologram is chosen and the acquired intensity at the corresponding pixels is integrated. Afterwards the hologram is erased and again the same wavelength is used to write the second hologram. Now the readout wavelength is detuned in steps of $\Delta\lambda=0.025$ nm. Again the reconstructed holograms are detected by the CCD and the intensity in the rectangular part is integrated. All obtained intensities are normalized to the Bragg-case. The dotted curve in Fig. (11) shows the experimental results for the normalized intensity as a function of readout wavelength-detuning, that agree very well to the calculated solid line in the same Figure. From the calculation the detuning parameter is found to be $\Delta\lambda=0.18$ nm, which means that we can theoretically multiplex two holograms, without cross-talk, that have a wavelength separation of $\Delta\lambda$.

We record three holograms sequentially with a wavelength separation of $\Delta\lambda=2$ nm. The first hologram is written at 818 nm within a writing time of 60 s. Then the laser is tuned to 820 nm and the second hologram is written in 50 s. Now again the laser is tuned, to 822 nm and the writing time is set to 40 s. After writing, the laser is tuned to 818 nm again and the first

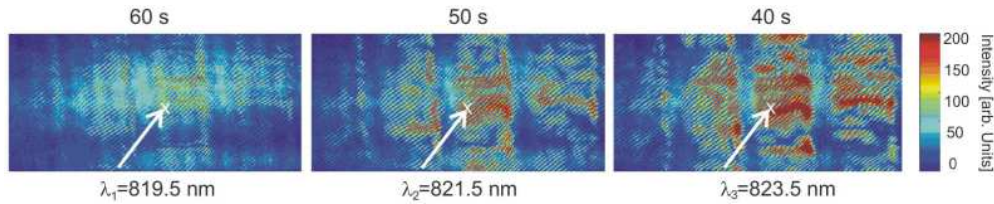


Fig. 12. Interference patterns obtained in one cycle of sequential multiplexing of three holograms. The left hologram is written in 60 s at 819.5 nm. The writing time of the hologram in the middle is set to 50 s, the wavelength being 821.5 nm. The hologram on the right is written in 40 s at a wavelength of 823.5 nm. The marked points can also be found in Fig. (13).

hologram is read out. The reconstructed object beam interferes on the CCD chip with the interference beam and the fringes are acquired. This is repeated for the remaining two holograms, before the multiplexed grating structure is erased. In the second recording cycle the wavelengths are shifted for 0.1 nm to 818.1 nm, 820.1 nm and 822.1 nm. Repeating this procedure 20 times leads to 60 interference patterns that again are analyzed like before. Three interference patterns that have been acquired during one recording cycle are shown in Fig. (12). As the holograms are multiplexed with a very simple approach of decreasing writing times, their diffraction efficiencies differ. Holograms written earlier have lower diffraction efficiencies as they are partially erased when other holograms are written. This degrades their diffraction efficiency as can be seen in Fig. (12). While the first hologram has the lowest intensity the hologram that has been last written has the highest one. The same can be recognized in Fig. (13) that shows the intensity modulation at one certain pixel position. The maximum intensity between 818 and 820 nm, that is the wavelength-range that has been written first, is lower compared to the rest. The intensity is higher for the middle-part (820-822 nm) and is the highest between 822 and 824 nm. The marked points in Fig. (13) correspond to the marked points in the interference patterns of Fig. (12). Using a recording schedule for sequential multiplexing as described in [44–46] the diffraction efficiencies of the holograms could be equalized. This has not been done in our simple proof of principle experiment.

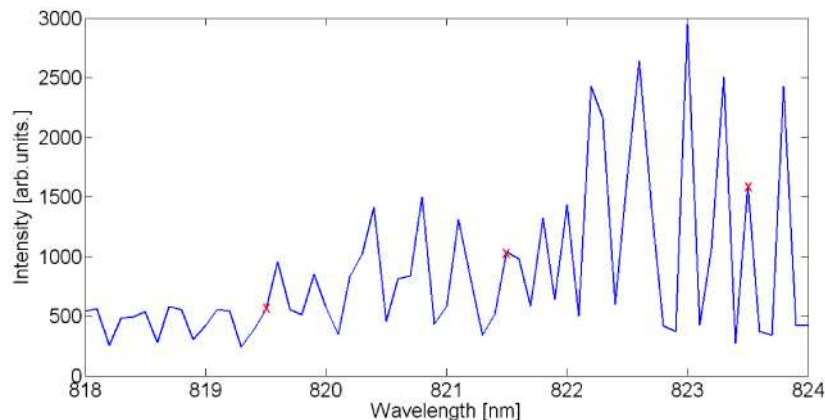


Fig. 13. Intensity modulation at pixel (400,200). The marked points correspond to the marked points in the interference patterns of Fig. (12).

In the next evaluation step the intensity modulation is again inversely Fourier-transformed and the depth-information at this pixel position is obtained. The results for the entire reconstructed image can be seen in Fig. (14). Again the depth of the sample is clearly reconstructed except for the third step at a path length difference of around $z=1100 \mu\text{m}$. This

is due to an inhomogeneity of the light distribution on our sample. From Fig. (12) it can be seen that the object beam is not perfectly incident on all steps and the major intensity is on the first two steps. This degrades the signal strength of the third step. Another factor that leads to errors is the used recording schedule. The intensity modulation of Fig. (13) shows that the intensity maxima in the modulation depend on their wavelength. This is caused by the mentioned difference of their diffraction efficiencies that depend on their writing order. This leads to additional noise decreasing the quality of the reconstruction.

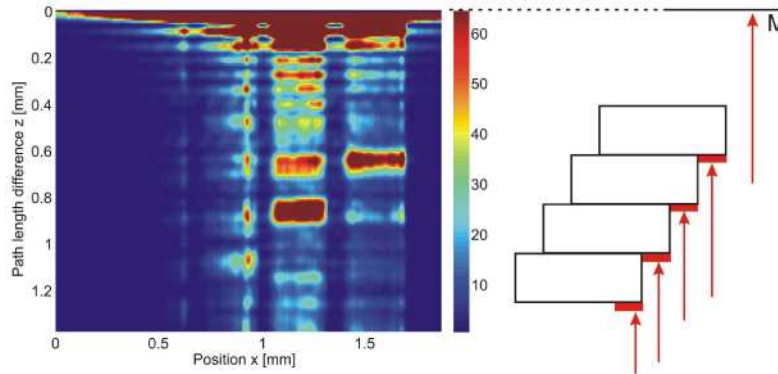


Fig. 14. Reconstructed image with three sequentially multiplexed holograms (left). Sample (right).

Nevertheless the result shows that the multiplexed storing does not affect the result of our experiment too much, but that it improves the setup.

3. Discussion

This third step of our proof of principle studies confirms, that it will be possible to improve the storage capability of the system again, using simultaneous wavelength-multiplexing. Consequently, our results demonstrate that the acquisition of high resolution 3D-images with a single laser shot will be possible by the usage of an appropriate light source providing a comb of simultaneously emitted wavelengths. As the multiplexed holograms have to be readout sequentially, another source has to be used for reconstruction. As the acquisition time is reduced to the writing time of the holograms the photorefractive build-up time of the crystal plays an important role. For practical applications, the writing time in our experiments is too long. A choice of another crystal will allow faster recording. It is well known, that 45°-cut Rh:BaTiO₃ crystals show faster response [47], and that elevated temperature enhances the photorefractive properties of Rh:BaTiO₃ crystals [48].

The research in the last few years concentrated on the photorefractive effect in tin-hypothiodiphosphate Sn₂P₂S₆ [49] which is a promising material, showing very fast response. It was recently reported, that Bi doped Sn₂P₂S₆ crystals show build-up times of some ms, being the fastest value reported for crystals operating in the near-infrared region [50].

Using very fast crystals and an appropriate comb-laser will lead to a very fast acquisition of 3D-image information within one single laser shot. This may be an important step towards a scanning free recording technique that overcomes several problems from which biomedical imaging suffers.

4. Conclusions

A new method for depth-resolved photorefractive holographic imaging is introduced. The technique is a combination of full-field swept-source optical coherence tomography and photorefractive holography. It promises extremely short acquisition times for a complete three dimensional (3D) image. Our first proof of principle results demonstrate the potential of our concept for scanning free recording of a data set, that bears all necessary information to

reconstruct the whole 3D information when a comb laser is used for wavelength multiplexing. This will allow storing the data within one single laser shot.